Efficacy and Toxicity Related to Treatment of Hepatocellular Carcinoma with ^{90}Y-SIR Spheres: Radiobiologic Considerations

Lidia Strigari[1], Rosa Sciuto[2], Sandra Rea[2], Livio Carpanese[3], Giuseppe Pizzi[3], Antonella Soriani[1], Giuseppe Iaccarino[1], Marcello Benassi[1], Giuseppe Maria Ettorre[4], and Carlo Ludovico Maini[2]

[1]Laboratory of Medical Physics and Expert Systems, Regina Elena National Cancer Institute, Rome, Italy; [2]Department of Nuclear Medicine, Regina Elena National Cancer Institute, Rome, Italy; [3]Department of Radiology, Regina Elena National Cancer Institute, Rome, Italy; and [4]Department of General Surgery and Liver Transplantation, Azienda Ospedaliera San Camillo-Forlanini, Rome, Italy

Radioactive ^{90}Y-selective internal radiation (SIR) sphere therapy is increasingly used for the treatment of nonresectable hepatocellular carcinoma (HCC). However, the maximum delivered dose is limited by severe injury to the nontarget tissue, including liver parenchyma. Our study aimed to implement radiobiologic models for both tumor control probability (TCP) and normal-tissue complication probability (NTCP) to describe more effectively local response and the liver toxicity rate, respectively. **Methods:** Patients with documented HCC, adequate bone marrow parameters, and regular hepatic and pulmonary function were eligible for the study. Patients who had pulmonary shunt greater than 20% of ^{99m}Tc-labeled macroaggregated albumin or any uncorrectable delivery to the gastrointestinal tract, reverse blood flow out of the liver, or complete portal vein thrombosis were excluded. Patients received a planned activity of the ^{90}Y-SIR spheres, determined using the empiric body surface area method. The dose distribution was determined using posttreatment (3-dimensional) activity distribution and Monte Carlo dose voxel kernel calculations, and the mean doses to healthy liver and tumor were calculated for each patient. Response was defined according to Response Evaluation Criteria in Solid Tumors (RECIST) and recommendations of the European Association for the Study of the Liver (EASL). Criteria were used to assess possible liver toxicities. The parameters of TCP and NTCP models were established by direct maximization of the likelihood. **Results:** Seventy-three patients were treated. With an average dose of 110 Gy to the tumor, complete or partial response was observed in 74% and 55% of patients according to the EASL guideline and RECIST, respectively, and the predicted TCPs were 73% and 55%, respectively. With a median liver dose of 36 Gy (range, 6–78 Gy), the ≥grade 2 (G2), ≥grade 3 (G3), and ≥grade 4 (G4) liver toxicities were observed in 32% (23/73), 21% (15/73), and 11% (8/73) of patients, respectively. The parameters describing the ≥G2 liver toxicity data using the NTCP model were a tolerance dose of the whole organ leading to a 50% complication probability of 52 Gy (95% confidence interval, 44–61 Gy) and a slope of NTCP versus dose of 0.28 (95% confidence interval, 0.18–0.60), assuming $n = 1$. **Conclusion:** The radiobiologic approach, based on patient-specific dosimetry, could improve the ^{90}Y-microsphere therapeutic approach of HCC, maintaining an acceptable liver toxicity.

Key Words: hepatocellular carcinoma; ^{90}Y; intrahepatic arterial therapy

J Nucl Med 2010; 51:1377–1385
DOI: 10.2967/jnumed.110.075861

Hepatocellular carcinoma (HCC) is a malignant epithelial tumor arising from parenchymatous liver cells (*1*). Patients with localized HCC (involvement of a single lobe and absence of vascular invasion or extrahepatic disease) are generally evaluated for the potentially curative therapeutic options of either partial hepatectomy or orthotopic liver transplantation. In contrast, more than 50% of patients underwent palliation of symptoms with external-beam radiotherapy (EBRT), and only 20% experienced significant tumor shrinkage (*2*).

These data suggest that HCC is radioresistant. However, the delivered dose is limited by severe injury to the surrounding tissue, including the liver parenchyma and duodenum (*3–5*). Given the limited efficacy of nonsurgical treatment, several techniques have been proposed to deliver targeted tumor radiation by means of radiopharmaceuticals for HCC treatment. In particular, radioactive ^{90}Y-microsphere therapy is increasingly used, and specific recommendations have been published (*6*).

Recently, some authors have applied radiobiologic principles to evaluate the biologic effect induced by therapies, with different time distributions of radiation. In particular, the linear-quadratic model has been extended to radionuclide therapy, including the biologic effective dose (BED) concept, which represents the dose producing the same biologic effect

Received Feb. 8, 2010; revision accepted Jun. 10, 2010.
For correspondence or reprints contact: Lidia Strigari, Laboratory of Medical Physics and Expert Systems, Regina Elena National Cancer Institute, Via E. Chianesi, 53, 00144 Rome, Italy.
E-mail: strigari@ifo.it

obtained under different irradiation conditions (*7–9*). The aim of this study was to apply 2 radiobiologic models, based on dosimetric and clinical data from a retrospective study, to adequately predict the clinical results on efficacy and toxicity of ^{90}Y-selective internal radiation (SIR) sphere (SIRT Medical Limited; www.sirtex.com) treatment in HCC.

On the basis of posttreatment 3-dimensional activity distribution and Monte Carlo dose voxel kernel calculations, the dose distribution was used to calculate the mean dose to healthy liver and tumor in each patient.

Moreover, radiobiologic models for both tumor control probability (TCP) and normal-tissue complication probability (NTCP) were implemented to interpret the local response and liver toxicity rate in our cohort.

MATERIALS AND METHODS

Inclusion Criteria

All patients were selected according to strict inclusion and exclusion criteria and were asked to give informed consent. Eligible patients were older than 18 y, with measurable unresectable disease predominately involving the liver, adequate bone marrow (granulocytes $>$ 1,500/mL; platelets $>$ 60,000/mL), hepatic (total bilirubin $\leq$ 2.0 mg/dL) serum glutamic oxaloacetic transaminase or serum glutamic pyruvic transaminase or alkaline phosphatase less than 5 times the upper limit of normal, pulmonary function (forced expiratory volume in 1 s $>$ 1 L), and no contraindications to angiography and selective visceral catheterization.

Absolute contraindications included pulmonary shunt greater than 20% of ^{99m}Tc-labeled macroaggregated albumin (^{99m}Tc-MAA) or any uncorrectable delivery to the gastrointestinal tract, reverse blood flow out of the liver, or complete portal vein thrombosis.

Radioactive Material

^{90}Y is a pure β-emitter, which decays to stable ^{90}Zr, with an average energy of 0.94 MeV and a half-life of 2.67 d (64.2 h). It is produced by neutron bombardment of ^{89}Y in a commercial reactor, yielding ^{90}Y β-radiation, with a mean tissue penetration of 2.5 mm and a maximum range of 1.1 cm. ^{90}Y that had been permanently embedded within resin structures (SIR spheres) was used for patients with the approval of the Food and Drug Administration. Each resin sphere has a diameter of 32 ± 10 μm, causing terminal arterioles within the tumor to be permanently embolized. A standard dose of ^{90}Y resin microspheres is 2 GBq, containing approximately 50 million microspheres (range, 40–80 million), with an activity per microsphere estimated to be 50 Bq. A maximum of 0.4% of administered ^{90}Y activity is free from the resin spheres according to the SIR spheres manual (*10*).

Administered Activity and Dosimetry

The administered activity of the ^{90}Y-SIR spheres was determined using the body surface area (BSA) empiric method given in the user's manual (*10*):

$$A(\text{GBq}) = (\text{BSA} - 0.2) + V_{\text{tumor}}/V_{\text{liver}}, \qquad \text{Eq. 1}$$

where V_{tumor} and V_{liver} are the volume of tumor and total liver, respectively, and BSA (m^2) is calculated as 0.20247 × height $(m)^{0.725}$ × weight $(kg)^{0.425}$.

This activity was used to treat the entire liver in 35 patients. A lobar approach was used in 38 of 73 patients. The right lobe was treated in 35 patients and the left in 3 patients. The activity was calculated considering the lobe volume in Eq. 1. The total delivered activity was reduced by 20% and 40% in patients with lung shunt between 10% and 15% or 15% and 20%, respectively. Accordingly, the dose was applied intraarterially on the treatment date, usually 10–14 d after obtaining the screening arteriography, either to the entire liver or to a single lobe.

Hepatic Angiography

An angiogram was obtained to assess hepatic vasculature, determine the appropriate catheter position for treatment, and identify any collateral vessels that would result in inadvertent microsphere deposition to the gastrointestinal tract. To prevent nontarget embolization, the gastroduodenal and right gastric arteries were prophylactically embolized in all patients. Embolization of vessels to create flow redistribution was not performed in any patient (i.e., embolization of accessory right or accessory left hepatic arteries to redistribute flow).

Imaging

All 73 patients were evaluated via chest, abdomen, and pelvic CT scans to detect extrahepatic metastases and to determine liver tumor location, size, and number. All scans were obtained with 3-mm slices.

After embolization of collateral vessels, ^{99m}Tc-MAA scans (anterior or posterior planar scans of lungs and abdomen and SPECT acquisition of abdomen) were obtained (within 30 min after embolization) to detect any unobserved gastrointestinal flow and estimate the percentage of injected activity that may shunt to the lungs. Therefore, pretherapy imaging was used to determine the liver–lung shunt.

Posttherapy (bremsstrahlung ^{90}Y-microspheres) planar and tomographic images were obtained to study the radioactivity distribution within 6 h after ^{90}Y injection. The SPECT scan was acquired using a triple-head γ-camera (Irix; Philips) equipped with a standard medium-energy general-purpose collimator. A wide window (from 55 to 245 keV) was used; 120 frames of 25 s were acquired using an elliptic orbit in a 128 × 128 image matrix with a magnification of 1.42.

Image Fusion, Image Quantification, and Dosimetry

Transaxial, coronal, and sagittal slices were reoriented with respect to the canthomeatal plane and reconstructed by an iterative method.

CT and SPECT images were registered and fused using a dedicated software program (Syntegra; Philips). A typical activity distribution using ^{99m}Tc-MAA and posttherapy bremsstrahlung microsphere images after hepatic embolization are shown in Figures 1A and 1C, respectively. Typical target regions of interest (ROIs) (tumor and liver) delineated on an axial CT slice are shown in Figure 1B.

Attenuation correction was performed using an ellipse determination (based on an automated threshold of about 10% maximum count), with a constant linear attenuation coefficient of 0.11 cm^{-1} using the Chang method. No scatter correction was performed.

The patient–lesion calibration factor was obtained by determining the ratio between the net administered activity (i.e., the difference between the activity—transferred in the V vial—to be delivered and the residual activity after the angiographic procedure, taking into account the physical decay) and total counts of

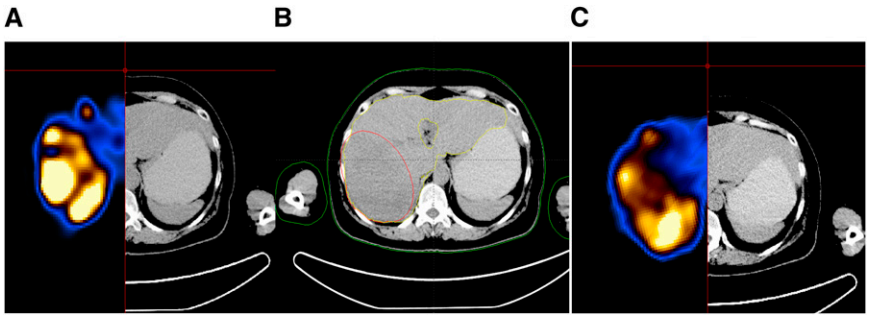

FIGURE 1. Typical activity distribution after hepatic embolization using ^{99m}Tc-MAA (A) and posttherapy bremsstrahlung ^{90}Y-microsphere images (C) fused with CT images (B). Typical target ROIs (tumor and liver) are delineated on axial CT slice (B).

all voxels included in the total liver ROI after background subtraction. The absorbed dose was obtained using in-house software by the convolution of the activity matrix from SPECT bremsstrahlung images and the dose voxel kernel value precalculated in water by Monte Carlo simulation, as described elsewhere (*11*). We observed 1, 2, 3, and more lesions in patients 21, 8, 6, and 38, respectively, and in each patient the tumor was identified by the largest lesion. Tumor and normal-liver ROIs were manually delineated by a radiologist or nuclear medicine physician (Fig. 1). The in-house software, developed using assembler language and installed on a high-performance personal computer, allowed us to calculate the dose volume histograms (DVHs), from which the mean dose to lesion and normal liver was obtained for each patient.

The time–activity curves for the source organs (liver and, in the case of a shunt, lungs, gastroduodenal tract, etc.) were supposed to decrease because of the physical decay only. The mean dose to lungs was calculated assuming a uniform microsphere distribution.

The tumor–to–normal-liver activity ratio (TNR) was calculated as:

$$\mathrm{TNR} = \frac{\text{total tumor counts}}{\text{total hepatic counts} - \text{total tumor counts}}. \qquad \text{Eq. 2}$$

Tumor Response

Response was defined according to Response Evaluation Criteria in Solid Tumors (RECIST) (*12*) and recommendations of the European Association for the Study of the Liver (EASL) (*13*), using World Health Organization criteria and taking into account tumor necrosis recognized by nonenhanced areas (Table 1).

Generally, CT may require 4–8 mo to reveal full response after ^{90}Y-SIR therapy (*14*); thus, only patients with an adequate minimum follow-up were included in this analysis.

Toxicity

Patients were followed closely until all acute toxicities were resolved, or at least every 2 wk for 6 wk, then monthly for 3 mo to observe the possible radiation hepatitis or other toxicities. The Common Terminology Criteria for Adverse Events (version 4; National Cancer Institute, Cancer Therapy Evaluation Program) were used as appropriate, according to the severity of the liver toxicity (Table 2).

Radiobiologic Models

The radiobiologic models, based on the linear-quadratic model, have been largely used to describe the surviving fraction (sf) of cells in the tissue exposed to a total radiation dose D. Recently, these models have been applied to systemic therapy (*9*).

The BED delivered to target and liver was calculated as follows:

$$\mathrm{BED} = \mathrm{D} + \mathrm{D}^2 \frac{\lambda}{(\mu+\lambda)} \frac{1}{\alpha/\beta}, \qquad \text{Eq. 3}$$

where D is expressed in Gy, α and β are tissue-specific parameters related to cell radiosensitivity (expressed in Gy^{-1} and Gy^{-2}, respectively), μ is a parameter incorporating the repair of sublethal radiation damage and $\mu = \ln(2)/T_{1/2,\mathrm{rep}}$ (expressed as h^{-1}) is the repair half-time of sublethal damage, and λ is the biologically effective decay constant $\lambda = \ln(2)/T_{1/2,\mathrm{phys}}$ (expressed as h^{-1}). The α-to-β ratio was equal to 10 and 2.5 Gy for tumor and normal liver, respectively (*15*).The $T_{1/2,\mathrm{rep}}$ was 1.5 and 2.5 h for tumor and normal liver, respectively (*16*).

The sf can be written as follows:

$$\mathrm{sf} = \times\exp\{-[\alpha \times \mathrm{BED}]\}. \qquad \text{Eq. 4}$$

The TCP, using the linear-quadratic model incorporating Poisson's law, can be written as:

$$\mathrm{TCP(D)} = \exp[-\mathrm{N}_0 \times \mathrm{sf(BED)}], \qquad \text{Eq. 5}$$

where N_0 is the initial number of clonogenic cells.

To take into account the inhomogeneity in the population sensitivity and density of clonogenic cells, the TCP can be written as follows:

TABLE 1. Criteria for Assessment of Response to ^{90}Y-Microsphere Treatment

Response	Criteria	
	EASL	RECIST
Complete	Disappearance of lesion or total necrosis	Disappearance of lesion
Partial	≥50% decrease or ≥30% necrosis	≥30% decrease
Stable disease	<50% decrease or <25% increase	<30% decrease or <20% increase
Progressive disease	≥25% increase or appearance of new lesions	≥20% increase or appearance of new lesions

TABLE 2. Criteria for Assessment of Liver Toxicity after ^{90}Y-SIR Treatment

Grade	Description
1	Mild; asymptomatic or mild symptoms; clinical or diagnostic observations only; intervention not indicated
2	Severe or medically significant but not immediately life-threatening; mild encephalopathy; reversal or retrograde portal vein flux associated with varices or ascites; hospitalization or prolonged hospitalization indicated; disabling; limiting self-care activities of daily living.
3	Hepatic coma, encephalopathy (life-threatening consequences); urgent intervention indicated.
4	Death related to advent averse.

Descriptions are taken from Common Terminology Criteria for Adverse Events.

$$TCP(D) = \exp\left(-\sum_i \eta_i \times N_0 \times sf(BED)\right), \quad \text{Eq. 6}$$

where

$$\eta_i = \frac{1}{\sqrt{2\pi}}\frac{1}{\sigma_{\ln(N)}}\exp\left\{-\frac{1}{2}\left(\frac{\ln(N_i) - \ln(N_0)}{\sigma_{\ln(N)}}\right)^2\right\} \quad \text{Eq. 7}$$

is the fraction of cells obtained from gaussian distributions of ln (N_i) values, with a mean value of $\ln(N_0)$ and an SD of $\sigma_{\ln(N)}$ (*17*).

A modified formalism of the NTCP model for the treatment of HCC, based on the Lyman–Burman Kutcher model, was used to evaluate specific radiobiologic parameters.

To compare the doses delivered during SIR procedures and EBRT, the adsorbed dose may be converted to an equivalent dose (EQ2) delivered at 2 Gy/fraction (the typical dose per fraction used in conventional EBRT), using the following equation (*18*):

$$EQ2 = \frac{BED}{1 + d/(\alpha/\beta)} = \left[D + D^2\frac{\lambda}{(\mu + \lambda)}\frac{1}{(\alpha/\beta)}\right]\frac{1}{1 + d/(\alpha/\beta)}, \quad \text{Eq. 8}$$

where α/β = 2.5 and 10 Gy for liver and tumor, respectively.

The NTCP was expressed as:

$$NTCP(t) = \frac{1}{\sqrt{2\pi}}\int_{-\infty}^{t}\exp\left(-\frac{s^2}{2}\right)ds, \quad \text{Eq. 9}$$

where s is a parameter defined as:

$$s = \frac{1}{m \times TD_{50}}(EQ2 - TD_{50}), \quad \text{Eq. 10}$$

where m is the slope of NTCP versus dose and TD_{50} is the tolerance dose of the whole organ leading to a 50% complication probability.

The full formulation of the Lyman–Burman Kutcher model includes another parameter, n, to convert an inhomogeneous into a homogeneous equivalent dose distribution. The values of this parameter range from zero (for a serial organ) to unity (for a parallel organ, such as the liver). In this article, we assumed n = 1 for liver (*19*).

Maximum-Likelihood Estimation

The standard BSA method used to determine the administered activity produced a wide-range dose to both lesions and liver.

The model parameters were established by direct likelihood maximization of the following equation:

$$L(m, TD_{50}(1)) = \sum_{i=1}^{N}\left[\ln(p_i)^{R_i} + \ln(1 - p_i)^{1-R_i}\right]. \quad \text{Eq. 11}$$

A probit model was assumed for the probability (p_i) of ≥grade 2 (G2) liver toxicity in the i-th patient:

$$p_i = p(m, TD_{50}(1); t_i) = NTCP(t_i), \quad \text{Eq. 12}$$

and all model parameters were adjusted to maximize the probability of predicting complications for those patients who did or did not experience liver toxicity (R_i = 1 or 0, respectively). In particular, the NTCP curve was calculated considering all ≥G2 liver toxicity as a complication.

A probit model was also assumed for $\pi = TCP(t_i)$, and model parameters were adjusted to maximize the probability of predicting the tumor control using both RECIST and EASL criteria.

For binomially distributed data, the log likelihood for the entire data was maximized by means of a in-house optimization package written in Visual Basic (Microsoft), already used by our group (*20*).

The observed endpoint (toxicity or tumor control) was used as truth—that is, the gold standard for nonparametric clustered receiver-operating-characteristic (ROC) analysis—to evaluate the predictive utility of a modified NTCP–TCP model (*21*). By comparing observed and calculated data, the true-positive and false-positive ratios were plotted in the form of an ROC curve. When a perfect correlation of the predicted versus observed control or ≥G2 liver toxicity was found, the area under curve (AUC) was 1. Random assignment of outcome led to a ROC AUC of 0.5. The goodness of fit was assessed using ROC AUC and its 95% confidence interval (CI).

RESULTS

Patients and Tumors

From January 2007 to July 2009, 73 patients (58 men, 15 women) with HCC lesions were treated with ^{90}Y-microspheres and retrospectively analyzed to assess tumor and normal-liver tissue dose. Median age was 66 y (range, 41–84 y).

On the basis of the Child–Pugh classification (*22*), 58 patients were Child–Pugh A, 13 Child–Pugh B, and 2 Child–Pugh C.

Tumor volumes (indicating the single or largest lesion for each patient) ranged from 2 to 1,932 cm^3 (median, 100 cm^3),

TABLE 3. 0th (Minimum), 25th, 50th (Median), 75th, and 100th (Maximum) Percentiles of Dosimetric Data

Parameter	Percentile				
	0	25	50	75	100
Injected activity (GBq)	1.0	1.5	1.7	1.9	2.3
Tumor–to–normal-tissue ratio	1.7	2.6	2.7	3.3	6.0
Lung shunt (%)	2%	5%	5%	10%	19%
Mean dose to liver/injected activity (Gy/GBq)	3.2	13.4	18.4	28.1	50.0
Mean dose to tumor/injected activity (Gy/GBq)	13.1	38.0	60.0	87.6	251.4
Mean dose to lungs/injected activity (Gy/GBq)	0.9	2.5	2.6	5.0	9.9

whereas the liver volumes ranged from 360 to 3,816 cm^3 (median, 1,783 cm^3).

Administered activities calculated using the standard BSA method ranged from 1.00 to 2.26 GBq, with a median of 1.73 GBq (Table 3).

Image Analysis

^{99m}Tc-MAA SPECT images of the abdomen after pretherapeutic embolization were sufficiently predictive of the ^{90}Y-SIR sphere distribution in more than 80% of patients. Moreover, before SIR treatment a further embolization was performed to avoid any flow redistribution during the time between the 2 embolization procedures. However, this topic deserves a separate paper.

Tumor Control and Toxicity

Complete response (CR), partial response (PR), stable disease, and progressive disease (PD) were seen in 1% (1/73), 53% (39/73), 43% (31/73), and 3% (2/73), respectively, using RECIST. According to the EASL guidelines, CR, PR, stable disease, and PD were seen in 26% (19/73), 51% (37/73), 20% (15/73), and 3% (2/73), respectively.

With a median liver dose of 36 Gy (range, 6–78 Gy) and an EQ2 of 33 Gy (3–90 Gy), ≥G2 liver toxicity was observed in 31% (23/73), ≥grade 3 (G3) liver toxicity in 21% (15/73), and ≥grade 4 (G4) liver toxicity in 11% (8/73) of the patients. With a median lung dose of 5 Gy (range, 1–15 Gy), no lung toxicity was observed. Gastroduodenal ulcers developed in 1 patient. No hematologic toxicity was observed in our cohort of patients.

Dosimetry and Radiobiologic Model

Analysis of the bremsstrahlung images of the 73 patients provided a median TNR of 2.7 (1.7–6.0). Median absorbed doses per unit activity were 18 (3–50) Gy/GBq to the nontumor liver and 60 (13–251) Gy/GBq to the tumor.

CR, PR, stable disease, and PD were observed in 19, 37, 15, and 2 patients, respectively, using the EASL guidelines, and according to RECIST, CR, PR, stable disease, and PD were found in 1, 39, 31, and 2 patients, respectively (Fig. 2).

CT scans of a patient before therapy and 5 mo after therapy are shown in Figure 3, together with the dose distribution and the DVH of total liver and target. In this patient, a PR (according to RECIST) and CR (according to the EASL guidelines) were registered, whereas no ≥G2 liver toxicity was observed.

The mean and median doses necessary to obtain CR using the EASL guidelines were 150 and 111 Gy, respectively, and the mean and median doses needed to obtain CR or PR were 110 and 97 Gy, respectively. For CR and PR using RECIST, the mean and median doses were 122 and 99 Gy, respectively.

The dose versus response type for the EASL guideline or RECIST is reported in Figure 4, and the calculated TCPs in terms of CR or PR are reported in Figure 5.

TCP curves were obtained from gaussian distributions of ln(N) values—the first (more radioresistant) with an α-value of 0.001/Gy, a mean value of $\ln(N_0)$ equal to 23, and an SD ($\sigma_{\ln(N)}$) of 18, and the second (less radioresistant) with an α-value of 0.005/Gy, an $\ln(N_0)$ of 6.9, and an $\sigma_{\ln(N)}$ of 6.2. The fit of the tumor control, based on RECIST and EASL criteria, indicates that 2 populations having 60% and 40% more radioresistant cells, respectively, were observed in our cohort.

Assuming all ≥G2 liver toxicity as a complication after ^{90}Y sphere treatment of HCC, the observed and predicted liver toxicity rate versus the mean BED to the liver was calculated and plotted in Figure 6, with a 95% CI. The parameters resulting from fittings to clinical toxicity data were a TD_{50} of 52 Gy (95% CI, 44–61 Gy) and an m of 0.28 (95% CI, 0.18–0.60), assuming $n = 1$. In Equation 3,

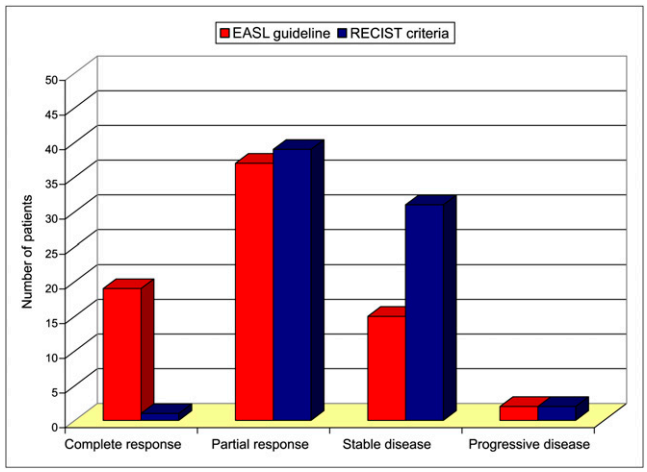

FIGURE 2. Tumor response observed in our patients according to EASL guideline and RECIST.

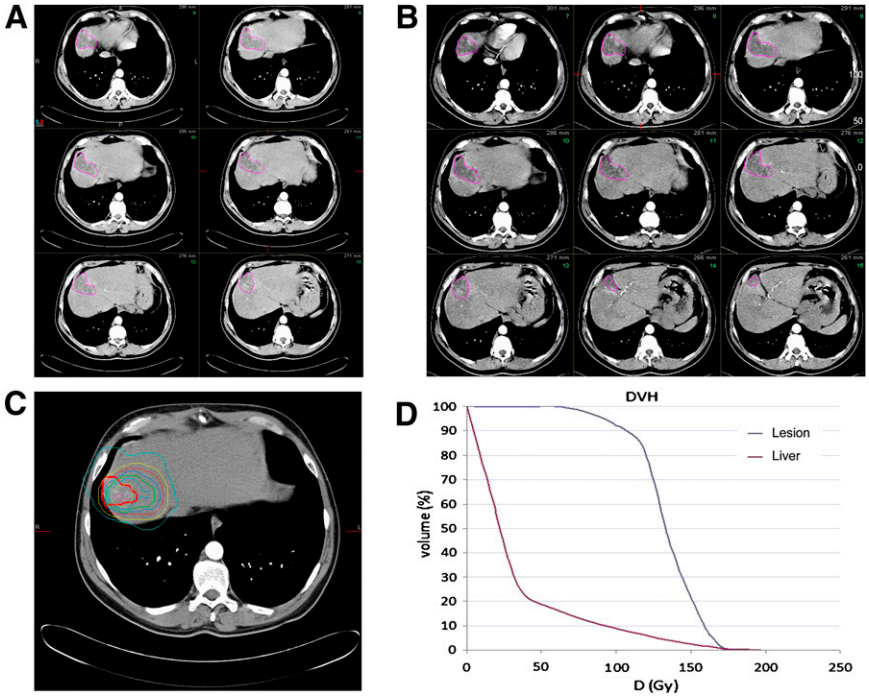

FIGURE 3. Pretherapy (A) and 5-mo posttherapy (B) CT scan of patient PR according to RECIST and CR according to EASL. (B) Evident necrosis with reduced peripheral enhancement is observed in place of HCC lesion (between V and VIII segments). Dose distribution (C) is shown over pretherapy CT scan. DVH of total liver and target is reported in D. Grade 1 (G1) liver toxicity was observed.

the tolerance BED of the whole organ leading to a 50% complication probability (BED50) was 93 Gy (95% CI, 79–110 Gy).

The predicted and observed toxicity in our group was 34%, and the AUC of the NTCP model was 0.612 (95% CI, 0.466–0.759). The predicted TCPs were 73% and 55%, and the AUCs of TCP models were 0.513 (95% CI, 0.340–0.685) and 0.594 (95% CI, 0.437–0.711) for RECIST and EASL criteria, respectively.

DISCUSSION

Selecting an appropriate treatment strategy for patients with HCC depends on careful tumor staging and assessment of the underlying liver disease.

Moreover, bremsstrahlung image quantification is still under evaluation. Recent publications have shown the possibility of using these images for dosimetry but after nontrivial important or significant calibration procedures and image corrections (*23*).

Because of the administration of ^{90}Y-SIR treatment, specific calibrator factors have been carried out for each patient to calculate the activity in each voxel of attenuation-corrected SPECT images, based on the net administered activity. The absorbed dose was obtained using in-house software through the convolution of the activity matrix from SPECT bremsstrahlung images and the dose voxel kernel estimation (*11*). DVHs were calculated from the liver and lesion ROIs delineated on CT images to obtain the mean dose. Dosimetric and clinical data were interpolated by TCP–NTCP models. In patients with HCC, the goal of all locoregional therapies (ablation or chemoembolization) is to obtain necrosis of the tumor, regardless of the shrinkage of the lesion. Even if an extensive tumor necrosis is achieved, this may not accompany a reduction in the dimension.

Regarding toxicity, substantial data are available on the acute and late side effects of ^{90}Y-SIR spheres in HCC patients. Symptoms including fatigue, nausea, and abdominal pain are quite common for patients undergoing ^{90}Y-SIR sphere therapy, who experience mild postemboli-

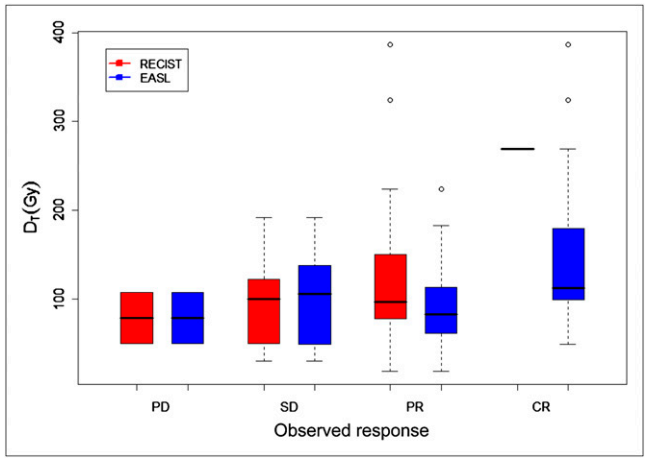

FIGURE 4. Lesion mean dose vs. tumor response type according to EASL guideline and RECIST. In box-and-whisker plot, central box represents values from lower to upper quartile (25th to 75th percentile). Middle line represents median. Vertical line extends from minimum to maximum value, excluding outside (circle) values, which are displayed as separate points. Outside values are values larger than upper quartile plus 1.5 times interquartile range.

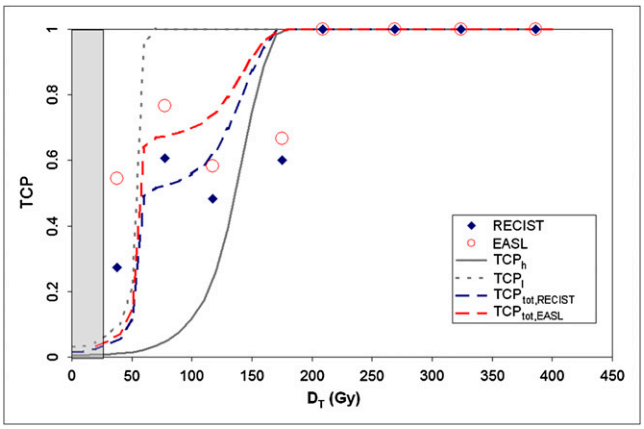

FIGURE 5. Tumor control probability vs. tumor mean dose according to EASL criteria and RECIST. Solid and dotted curves represent TCP for more (TCP_h) or less (TCP_l) radioresistant tumors, respectively, in our study. Upper ($TCP_{tot,EASL}$) and lower ($TCP_{tot,RECIST}$) dashed curves represent weighted sum of above population to describe tumor response according to EASL and RECIST, respectively. ♦ and ○ represent experimental data. Gray area indicate no lesions received dose lower than about 20 Gy. D_T = tumor dose.

zation syndrome on the day of treatment and for up to 3 d thereafter.

Radioembolization to nontarget organs can also cause other acute damage, resulting in gastrointestinal ulceration, pancreatitis, and radiation pneumonitis. The incidence of radiation effects could be minimized if meticulous angiographic techniques and dosimetry are used (*24*). Strict adherence to accepted limits on radiation dose (<30 Gy) to the lung prevents this complication (*25*). No lung toxicity was observed in our patients. Despite careful evaluation before treatment and attempts to reduce SIR sphere exposure, gastroduodenal ulcers did develop in 1 patient.

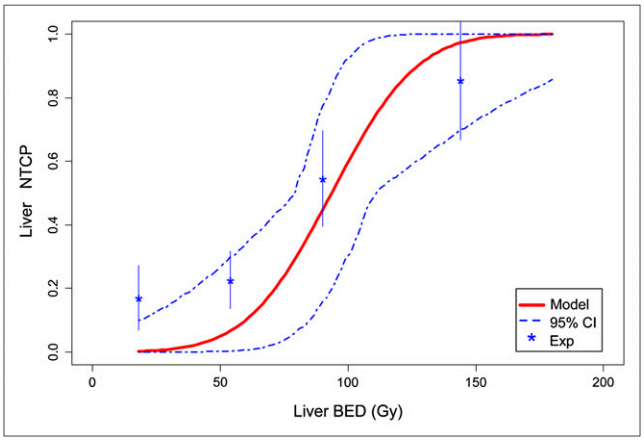

FIGURE 6. Normal-tissue complication probability of liver toxicity (solid line) vs. liver BED. Dashed line represents 95% CI. Vertical bars represent SD (caused by number of data in each group that created each point). Exp = experimental data.

A long-term sequela of ^{90}Y treatment may be radiation-induced liver disease (*26–29*). When the whole liver is exposed to external-beam radiation at a mean radiation dose of more than 40 Gy, more than 50% of patients develop liver dysfunction (*30*). Many other researchers have also reported tolerance doses for individual organs and ^{90}Y-SIR sphere therapy, but data concerning late liver toxicity are scarce. In particular, dose escalation in 10 patients showed that up to 138 Gy to the nontumorous liver by SIR treatment did not cause clinical radiation hepatitis (*31*). Moreover, 70 Gy by SIR treatment to the nontumorous part of the liver is tolerable in cirrhosis (*32*). Biopsies in 4 patients receiving up to 75 Gy by SIR treatment showed a minimal histologic effect in the healthy liver (*31*). When the normal-liver dose was estimated separately, the maximum average dose was 75 Gy, with up to 147 Gy delivered to the tumor (*33*). From their study of a dog model, Wollner et al. (*34*) estimated that the human liver can easily tolerate 100 Gy. Assuming all ≥G2 liver toxicity as a complication after ^{90}Y-SIR spheres treatment of HCC, and n = 1, the estimated parameters of the NTCP curve were a BED50 of 93 Gy and an m of 0.28. The value of the estimated BED50 is higher than the 72 Gy reported for late effect—that is, liver failure—by Emami et al. (*30*). Although factors other than dose distribution may be significant, this apparent discrepancy could be reconciled if the distribution of microspheres was more macroscopically nonuniform (*33*) because of the vasculature of the major vessels. Moreover, the fact that toxicity occurred within 4–6 mo after treatment in our series might be due to the high–dose-rate effect generated by SIR treatment, probably because the dose to liver is delivered in a shorter time (about 10 d) than in EBRT, producing early or premature vascular damage.

Moreover, our results are higher than those of Dawson et al. (*19*), who found a TD_{50} of 39.8 Gy (BED50 = 64 Gy), an m of 0.12, and an n of 0.97 for primary liver tumors treated at a dose fraction of 1.5 Gy. Furthermore, our parameters are lower in terms of BED50 but similar in terms of m and n to those obtained by Xu et al. (*35*) for primary liver patients with Child–Pugh A cirrhosis treated at a dose fraction of 4.6 Gy (TD_{50} = 40.5 Gy, BED50 = 115 Gy, m = 0.28, and n = 1.1). This difference might be because 21% (15/73) of our patients had pretreatment Child–Pugh B or C cirrhosis. From a radiobiologic point of view, these differences could be further explained by the fact that in the typical dose distribution delivered using ^{90}Y-SIR spheres the higher doses were received in smaller volumes, increasing the probability of cross-firing with a possible loss of biologic effect.

Regarding tumor control, the mean dose to the tumor may be predictive of final therapy outcome (i.e., cure) but may not be the best predictor of tumor response. Likewise, the average dose seems to be more adequate for parallel organs, such as the liver, capable of maintaining function when a limited part of an organ receives a higher dose.

Doses to the tumor higher than 110–120 Gy are able to obtain PR or CR (according to both criteria) in at least 50% of patients. All the values discussed above were higher than 100 Gy, which is the recommended target-absorbed dose for nonresectable HCC (*36*).

However, tumor response varies according to the criteria applied. In fact, according to the EASL guidelines or RECIST, a significant difference in the CR or PR was registered (i.e., in 74% or 55% of patients, respectively, using an average dose of 110 Gy). This difference could be because RECIST evaluates only 1-dimensional tumor measurements and disregards the extent of the necrosis, which is the objective of all locoregional therapy used for HCC, including ablation and intraarterial procedures such as chemoembolization. Considering that a multivariate analysis of survival clearly demonstrated that the complete tumor necrosis was associated with significantly better survival (odds ratio, 1.83; 95% CI, 1.1–3.1; $P = 0.020$) (*37*), the use of combined (size and necrosis) criteria might lead to a more accurate assessment of response to ^{90}Y radioembolization than criteria based on size alone (*38*).

Recently, Coldwell et al. (*39*) introduced the response based on ^{18}F-FDG PET—which demonstrated a high degree of response, compared with RECIST (CR or PR 91% vs. 47%), and appears to be well demonstrated by the survival of the patients in their series.

In our series, the CR or PR based on RECIST was similar to that reported by Coldwell et al. (*39*), whereas that based on the EASL guidelines was 77% for intermediate values with respect to the RECIST and ^{18}F-FDG PET criteria. Consequently, ^{18}F-FDG PET is expected to improve the assessment of tumor response. However, our study was based on CT/MR images and RECIST and EASL criteria, before the installation of 2 PET/CT devices at our institute.

Moreover, the behavior of the TCP curves suggests that the role of the inhomogeneity should be investigated, and DVH might be a valid method to assess the inhomogeneity of dose distribution; however, more advanced mathematic models still need to be applied (*40,41*). In addition, although the availability of a map of dose distribution allows correlations at the voxel level to be performed, the shrinkage of the tumor and the healthy remodeling of the liver could make a conclusive correlation more difficult.

The use of a more simplified model based on mean dose could provide robust results when the target dose distribution is sufficiently homogeneous and the liver can be considered a parallel organ (i.e., the liver failure probability increases with the liver mean dose). Assuming the same dosage to both tumor and liver, the BED for liver is higher than that for tumor. However, the angiographic approach, limiting liver involvement, decreases the mean dose to the healthy liver. Moreover, on the basis of these preliminary findings the TCP and NTCP models permit the outcome to be predicted and the activity giving the highest therapeutic gain to be calculated. When the expected NTCP of the liver is higher than the acceptable cutoff (generally 20%–30%), the use of a superselective approach or the possibility of multicycle treatments (*15*) should be carefully evaluated.

CONCLUSION

^{90}Y-SIR sphere therapy is a complex procedure that requires multidisciplinary management for safety and success. Our results support that a radiobiologic approach, based on patient-specific dosimetry, is a feasible and effective method to increase treatment efficacy sparing normal-tissue ^{90}Y therapy.

According to the NTCP–TCP model, new clinical protocols should be designed to improve the risk–benefit balance. Additional data on a larger cohort are required to improve the outcome prediction.

ACKNOWLEDGMENT

We thank Paula Franke for the English revision of the manuscript.

REFERENCES

1. Röcken C, Carll-McGrath S. Pathology and pathogenesis of hepatocellular carcinoma. *Dig Dis.* 2001;19:269–278.
2. Di Bisceglie AM, Rustgi VK, Hoofnagle JH, Dusheiko GM, Lotze MT. NIH conference: hepatocellular cancer. *Ann Intern Med.* 1988;108:390–401.
3. Lin DY, Lin SM, Liaw YF. Non-surgical treatment of hepatocellular carcinoma. *J Gastroenterol Hepatol.* 1997;12:S319–S328.
4. Cheng JC, Wud JK, Huanga CM, et al. Radiation-induced liver disease after radiotherapy for hepatocellular carcinoma: clinical manifestation and dosimetric description. *Radiother Oncol.* 2002;63:41–45.
5. Seong J, Park HS, Han KH, et al. Local radiotherapy for unresectable hepatocellular carcinoma patients who failed with arterial chemoembolization. *Int J Radiat Oncol Biol Phys.* 2000;47:1331–1335.
6. Kennedy A, Nag S, Salem R, et al. Recommendations for radioembolization of hepatic malignancies using yttrium-90 microsphere brachyterapy: a consensus panel report from the radioembolization brachytheraphy oncology consortium. *Int J Radiat Oncol Biol Phys.* 2007;68:13–23.
7. Dale RG. Dose-rate effects in targeted radiotherapy. *Phys Med Biol.* 1996; 41:1871–1884.
8. Dale R, Carabe-Fernandez A. The radiobiology of conventional radiotherapy and its application to radionuclide therapy. *Cancer Biother Radiopharm.* 2005;20: 47–51.
9. Strigari L, D'Andrea M, Maini CL, et al. Biological optimization of heterogeneous dose distributions in radionuclide direct therapy. *Med Phys.* 2006;33:1857–1866.
10. Sirtex Medical Limited. SIR-Spheres Training Program, Physicians and Institutions. Available at: http://www.sirtex.com/files/TRN-US-0320for20US1.pdf. Accessed August 3, 2010.
11. Strigari L, Menghi E, D'Andrea M, et al. Monte Carlo dose voxel kernel calculations of beta-emitting and Auger-emitting radionuclides for internal dosimetry: a comparison between EGSnrcMP and EGS4. *Med Phys.* 2006;33: 3383–3389.
12. Therasse P, Arbuck SG, Eisenhauer EA, et al. New guidelines to evaluate the response to treatment in solid tumors. European Organization for Research and Treatment of Cancer, National Cancer Institute of the United States, National Cancer Institute of Canada. *J Natl Cancer Inst.* 2000;92:205–216.
13. Bruix J, Sherman M, Llovet JM, et al. Clinical management of hepatocellular carcinoma: conclusions of the Barcelona-2000 EASL-conference. European Association for the Study of the Liver. *J Hepatol.* 2001;35:421–430.
14. Jakobs T. Radiologic follow-up of patients treated with SIRT. Paper presented at: Liver-Directed Radiotherapy with Microspheres: A Clinical Symposium; February 11–12, 2006; Barcelona, Spain.
15. Cremonesi M, Ferrari M, Bartolomei M, et al. Radioembolization with ^{90}Y-microspheres: dosimetric and radiobiological investigation for multi-cycle treatments. *Eur J Nucl Med Mol Imaging.* 2008;35:2088–2096.

16. Krishnan S, Lin EH, Gunn GB, et al. Conformal radiotherapy of the dominant liver metastasis: a viable strategy for treatment of unresectable chemotherapy refractory colorectal cancer liver metastases. *Am J Clin Oncol.* 2006;29:562–567.
17. Strigari L, D'Andrea M, Abate A, Benassi M. A heterogeneous dose distribution in simultaneous integrated boost: the role of the clonogenic cell density on the tumor control probability. *Phys Med Biol.* 2008;53:5257–5273.
18. Withers HR, Thames HD Jr, Peters LJ. A new isoeffect curve for change in dose per fraction. *Radiother Oncol.* 1983;1:187–191.
19. Dawson LA, Normolle D, Balter JM, et al. Analysis of radiation-induced liver disease using the Lyman NTCP model. *Int J Radiat Oncol Biol Phys.* 2002; 53:810–821.
20. Strigari L, Arcangeli G, Arcangeli S, Benassi M. A mathematical model for evaluating the incidence of acute rectal toxicity during conventional or hypo-fractionated radiotherapy courses for prostate cancer. *Int J Radiat Oncol Biol Phys.* 2009;73:1454–1460.
21. Obuchowski NA. Nonparametric analysis of clustered ROC curve data. *Biometrics.* 1997;53:567–578.
22. Child CG, Turcotte JG. Surgery and portal hypertension. In: Child CG, ed. *The Liver and Portal Hypertension.* Philadelphia, PA: Saunders; 1964:50–64.
23. Minarik D, Sjögreen Gleisner K, Ljungberg M. Evaluation of quantitative ^{90}Y-SPECT based on experimental phantom studies. *Phys Med Biol.* 2008;53:5689–5703.
24. Rhee TK, Omary RA, Gates V, et al. The effect of catheter directed CT angiography on yttrium-90 radioembolization treatment of hepatocellular carcinoma. *J Vasc Interv Radiol.* 2005;16:1085–1091.
25. Leung TW, Lau WY, Ho SK, et al. Radiation pneumonitis after selective internal radiation treatment with intra-arterial 90yttrium-microspheres for inoperable hepatic tumors. *Int J Radiat Oncol Biol Phys.* 1995;33:919–924.
26. Goin JE, Salem R, Carr BI, et al. Treatment of unresectable hepatocellular carcinoma with intrahepatic yttrium 90 microspheres: factors associated with liver toxicities. *J Vasc Interv Radiol.* 2005;16:205–213.
27. Thamboo T, Tan KB, Wang SC, et al. Extra-hepatic embolisation of Y-90 microspheres from selective internal radiation therapy (SIRT) of the liver. *Pathology.* 2003;35:351–353.
28. Ho S, Lau WY, Leung TW, et al. Partition model for estimating radiation doses from yttrium-90 microspheres in treating hepatic tumours. *Eur J Nucl Med.* 1996;23:947–952.
29. Ingold J, Reed G, Kaplan H, Bagshaw MA. Radiation hepatitis. *AJR.* 1965;93:200–208.
30. Emami B, Lyman J, Brown A, et al. Tolerance of normal tissue to therapeutic irradiation. *Int J Radiat Oncol Biol Phys.* 1991;21:109–122.
31. Gray B, Burton MA, Kelleher DK, et al. Selective internal radiation (SIR) therapy for treatment of liver metastases: measurement of response rate. *J Surg Oncol.* 1989;42:192–196.
32. Lau WY, Leung WT, Ho S, et al. Treatment of inoperative hepatocellular carcinoma with intra-arterial yttrium-90 microspheres: a phase 1 and 2 study. *Br J Cancer.* 1994;70:994–999.
33. Burton MA, Gray BN, Klemp PF, Kelleher DK, Hardy N. Selective internal radiation therapy: distribution of radiation in the liver. *Eur J Cancer Clin Oncol.* 1989;25:1487–1491.
34. Wollner I, Knutsen C, Smith P, et al. Effects of hepatic arterial yttrium-90 glass microspheres in dogs. *Cancer.* 1988;61:1336–1344.
35. Xu ZY, Liang SX, Zhu JRD, et al. Prediction of radiation induced liver disease by Lyman normal-tissue complication probability model in three-dimensional conformation radiation therapy for primary liver carcinoma. *Int J Radiat Oncol Biol Phys.* 2006;65:189–195.
36. Dancey JE, Shepherd FA, Paul K, et al. Treatment of nonresectable hepatocellular carcinoma with intrahepatic ^{90}Y-microspheres. *J Nucl Med.* 2000;41:1673–1681.
37. Sala M, Llovet JM, Vilana R, et al. Initial response to percutaneous ablation predicts survival in patients with hepatocellular carcinoma. *Hepatology.* 2004;40:1352–1360.
38. Keppke AL, Salem R, Reddy D, et al. Imaging of hepatocellular carcinoma after treatment with yttrium-90 microspheres. *AJR.* 2007;188:768–775.
39. Coldwell DM, Kennedy AS, Nutting CW. Use of yttrium-90 microspheres in the treatment of unresectable hepatic metastases from breast cancer. *Int J Radiat Oncol Biol Phys.* 2007;69:800–804.
40. Kutcher GJ, Burman C. Calculation of complication probability factors for non-uniform norma1tissue irradiation: the effective volume method. *Int J Radiat Oncol Biol Phys.* 1989;16:1623–1630.
41. Lyman JT, Wolbarst AB. Optimization of radiation therapy IV: a dose-volume histogram reduction algorithm. *Int J Radiat Oncol Biol Phys.* 1989;17:433–436.